BUNCH LENGTH MEASUREMENT AT THE FERMILAB A0 PHOTOINJECTOR USING A MARTIN-PUPLETT INTERFEROMETER*

Randy Thurman-Keup#, Raymond Patrick Fliller, Grigory Kazakevich (Fermilab, P.O. Box 500, Batavia, Illinois 60510)

Abstract

We present preliminary measurements of the electron bunch lengths at the Fermilab A0 Photoinjector using a Martin-Puplett interferometer on loan from DESY. The photoinjector provides a relatively wide range of bunch lengths through laser pulse width adjustment and compression of the beam using a magnetic chicane. We present comparisons of data with simulations that account for diffraction distortions in the signal and discuss future plans for improving the measurement.

INTRODUCTION

Application of Coherent Transition Radiation (CTR) diagnostics based on correlation techniques for bunch length measurements in the sub-millimeter range was proposed more than 10 years ago and numerous articles have been devoted to the problem, [1,2,3]. The diagnostic employs Transition Radiation (TR), [4], which is coherent at wavelengths approximately equal to or exceeding the bunch length. This technique suffers from a number of issues, some of which will be discussed in this paper.

The measurements in this paper were taken at the A0 photoinjector at Fermilab during 2007. Figure 1 is a schematic of the photoinjector as it existed at that time.

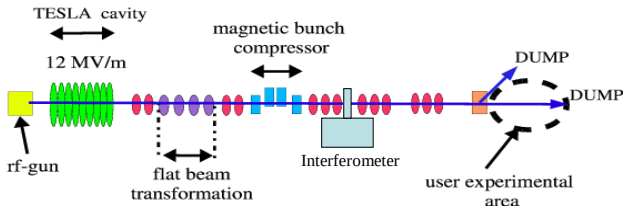

Figure 1: Schematic of the A0 photoinjector showing the main components. The interferometer is just downstream of the bunch compressor.

Beam is provided by a 1.3 GHz rf-gun with a CsTe photocathode. Typical charge is a few nC per micropulse. The micropulses are spaced by 1 μs and the overall rep rate is 1 Hz. The beam is accelerated via a TESLA 1.3 GHz SCRF cavity to energies around 16 MeV. A magnetic chicane does bunch compression of the beam just upstream of the interferometer with an expected compressed bunch length of 1-2 ps. The interferometer used for these measurements was obtained from DESY where it had also been used to make bunch length measurements. The thesis by Lars Frohlich [5] contains detailed descriptions of both the technique and the DESY measurements together with many references to previous work.

BUNCH LENGTH INTERFEROMETRY

Correlation between bunch length and spectrum

Interferometric bunch length measurements are possible because of the correlation between the bunch length and the spectral content of the CTR. This relationship is formally

$$I(\omega) = I_0(\omega)\cdot\left(N + N(N-1)\left|F(\omega)\right|^2\right) \qquad (1)$$

where $I_0(\omega)$ is the single particle spectrum, and the complex form factor, $F(\omega)$, is the Fourier Transform of the longitudinal charge distribution

$$F(\omega) = \frac{1}{Q}\int dz\,\rho(z)\,e^{-i\omega z} \qquad (2)$$

where the transverse contributions are small, provided the observation point is close to the emission axis, and have been ignored.

Notice that the intensity is a function of only the magnitude of $F(\omega)$ and as such, in general, an exact determination of the longitudinal charge distribution cannot be obtained. However, for certain simple shapes, such as Gaussians, the approximations necessary to obtain the phase values do a fairly good job of preserving the main parameters of the bunch, such as width.

Reconstruction of the phase

Determination of the phase of the complex form factor involves writing the form factor as a product of a term without complex zeros and a term that contains just the zeros.

$$F(\omega) = e^{i\varphi(\omega)} = e^{i\eta(\omega)}e^{i\xi(\omega)}$$

$$\varphi(\omega) = \eta(\omega) + \xi(\omega)$$

The phase of the first term, $\eta(\omega)$, is termed the 'minimal phase' and in fact contains most of the information for a variety of simple shapes such as Gaussians. It also happens that the minimal phase can be obtained from a Kramers-Kronig equation. The phase of the second term, however, is not obtainable from just the magnitude of the form factor and hence ϕ must be approximated by just η.

The imaginary part of η, η_i, is just the logarithm of the magnitude of F. The real part of η, η_r, is related by the Kramers-Kronig relation to the imaginary part

* Fermilab is operated by Fermi Research Alliance, LLC under Contract No. DE-AC02-07CH11359 with the United States Department of Energy.

keup@fnal.gov

$$\eta_r(\omega) = \frac{2\omega}{\pi}\int_0^\infty d\omega' \frac{\eta_i(\omega) - \eta_i(\omega')}{\omega^2 - \omega'^2}$$
$$= \frac{2\omega}{\pi}\int_0^\infty d\omega' \frac{\ln\dfrac{|F(\omega)|}{|F(\omega')|}}{\omega^2 - \omega'^2}$$

This provides at least part of the missing phase information, which can be combined with the magnitude to complete the complex form factor

$$F(\omega) = |F(\omega)|e^{i\eta_r} \propto \left|\sqrt{I(\omega)}\right| e^{i\frac{2\omega}{\pi}\int_0^\infty d\omega' \frac{\ln\frac{|\sqrt{I(\omega)}|}{|\sqrt{I(\omega')}|}}{\omega^2-\omega'^2}} \quad (3)$$

where, from Equation 1, $F(\omega) \propto \sqrt{I(\omega)}$ assuming the single particle spectrum is flat over the frequency range of interest (diffraction effects make this untrue as discussed in the next sections).

Diffraction effects in the CTR spectra

Diffraction effects have been discussed in a number of works [6,7,8]. In the last one, estimates were made of the systematic errors in determining the bunch length through the Fourier transform of the CTR spectra considering diffraction of the CTR due to the finite size of the TR screen. The diffraction distorts the TR angular distribution resulting in distortion of the CTR spectra. For CTR with wavelength, λ, the distortions become apparent at $\lambda\gamma > a$, $\lambda\gamma^2 > b$, where a is the TR screen radius, γ is the Lorentz factor, and b is the distance to the point of observation. Following [8] we consider the effect of the limited size of the OTR screen in the bunch length measurements at the A0 Photoinjector.

The angular distribution of the incoherent TR with frequency ω generated on the TR screen with radius a is expressed as, [8]:

$$\frac{d^2U}{d\omega d\Omega} = I(\omega,\theta) = 2\varepsilon_0 cR^2\left|\tilde{E}_x(\omega,\theta)\right|^2$$

where ε_0 is the permittivity of vacuum,

$$\tilde{E}_x(\omega,\theta) \approx \frac{e\omega^2}{(2\pi)^{3/2}\varepsilon_0\beta^2 c^3\gamma}\cdot\frac{e^{\frac{i\omega R}{c}}}{R} \times\int_0^a J_1\left(\frac{\omega\rho\sin\theta}{c}\right)K_1\left(\frac{\omega\rho}{\beta c\gamma}\right)\cdot e^{\frac{i\omega\rho^2}{2cR}}\rho d\rho$$

where $J_1(u)$ and $K_1(p)$ are the Bessel function first and second kind, respectively, and $R = b/\cos\theta$ is distance between the OTR screen center (the origin) and the point of observation. Figure 2 shows the TR angular distributions for various wavelengths calculated for the single electron having an energy of 15 MeV with a TR screen size of a = 12.5 mm and a distance between the TR screen and the detector of 250 mm.

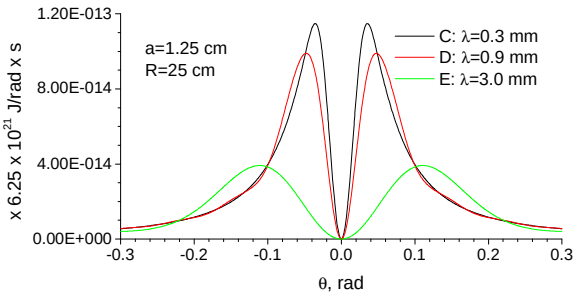

Figure 2: Angular distribution of the backward TR at 0.3 mm, 0.9 mm, and 3.0 mm wavelengths for 15 MeV electrons.

Figure 2 shows that the violation of the requirement $\lambda\gamma < a$ causes noticeable broadening of the angular distribution. For limited detector acceptance, this implies a distortion of the CTR spectra that depends on the bunch length.

Diffraction effects in the Bunch Length

CTR spectra were computed in assuming a Gaussian longitudinal distribution of the charge in a thread-like bunch. For small angles of observation the total CTR spectral power within the angle θ_0 is equal to, [6]:

$$I(\omega) = 2\pi N^2\int_0^{\theta_0} d\theta\left(e^{-\omega^2/2\sigma_\omega^2}\right)^2 I(\omega,\theta)\sin\theta\,.$$

Here N is the number of electrons in the bunch and σ_ω is σ of the bunch in the frequency domain. Calculated CTR spectra in 1 Hz bands with the current experimental acceptance limitations are shown in Figure 3 for several bunch lengths.

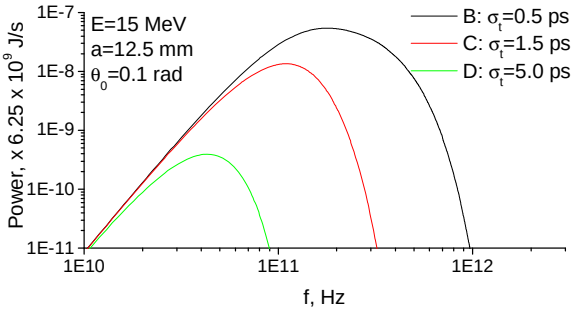

Figure 3: Calculated CTR spectra for 15 MeV, 1 nC bunch for different σ_t at a = 12.5 mm, θ_0 = 0.1 rad.

The calculations show that the diffraction effects noticeably shift the low frequency boundary of the CTR spectra to higher frequencies at limited size of the TR screen and limited detector acceptance. In fact these distortions of the CTR spectra lead to the "shortening" of the electron bunch length if it is computed using the inverse Fourier transform. Corresponding results are shown in Figure 4 for different σ_t values.

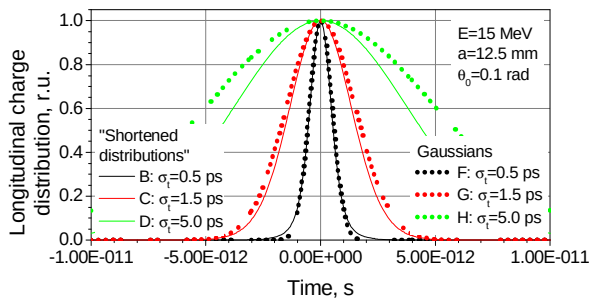

Figure 4: "Shortening" of the bunch length caused by diffraction. Curves *B, C, E* correspond to σ_t = 0.5, 1.5, 5 ps, corresponding to bunch lengths of approximately 0.3 mm, 0.9 mm and 3 mm, respectively.

Computed dependence of the "shortening" of the bunch length vs. the bunch σ_t is shown in Figure 5. The Systematic errors in determination of the bunch duration vs. the bunch σ_t are also plotted in this figure.

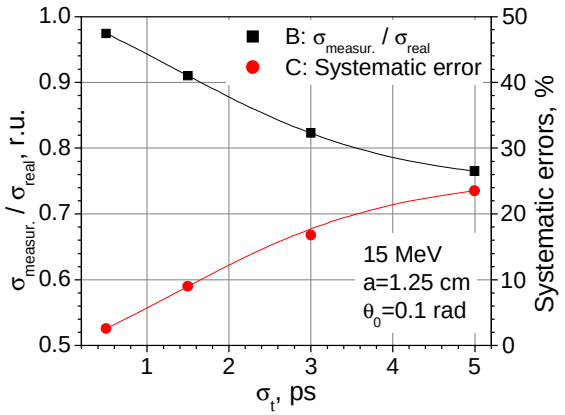

Figure 5: "Shortening" of the bunch length and the systematic errors caused by diffraction for correlation measurements using the A0 Photoinjector setup.

These plots show noticeable systematic errors in the bunch length caused by diffraction, if the distortion of CTR spectra is unaccounted for at longer bunch lengths. The effect is caused by a combination of the finite size of the TR screen (the Fraunhofer diffraction) and the finite acceptance of the detecting device (the Fresnel diffraction).

MARTIN-PUPLETT INTERFEROMETER

A Martin-Puplett interferometer is a polarizing type interferometer which in this case uses closely spaced wire grids for the polarizers and splitters (Fig. 6). The grids consist of 15 μm diameter gold-plated tungsten wires spced by 45 μm.

The CTR exits the beamline through a quartz window and is immediately collimated by a 200mm focal length off-axis parabolic mirror. Another flat mirror directs the light into the interferometer and through the horizontal input polarizer resulting in the following plane wave

$$\mathbf{E}(t) = E_0 \sin(\omega t)\mathbf{n}_h$$

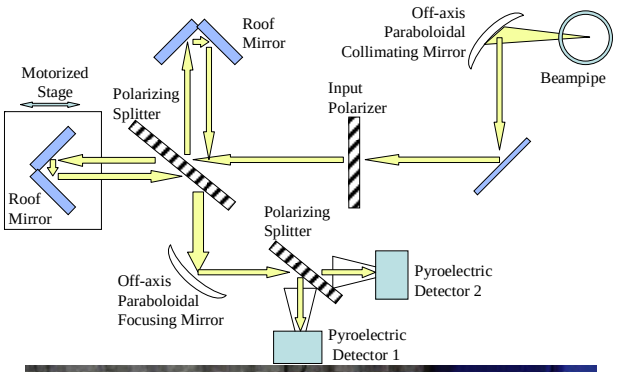

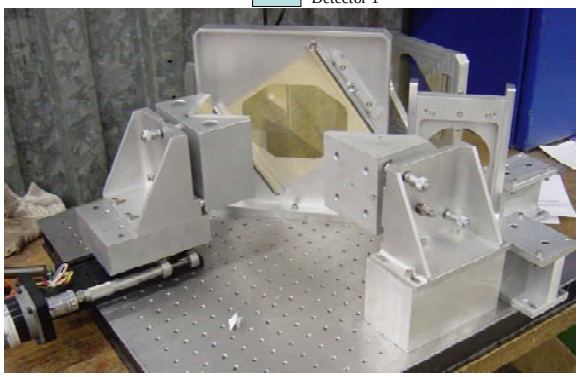

Figure 6: Schematic and photograph of interferometer. The large gold colored section in the photograph is the wire grid of the beam splitter for the two paths.

where $\mathbf{n}_h$ and $\mathbf{n}_v$ are horizontal and vertical unit vectors. This wave is split by the beam splitter, which is oriented diagonally, into the two polarizations

$$\mathbf{E}_1(t) = \frac{E_0}{2}\sin(\omega t)(\mathbf{n}_h + \mathbf{n}_v)$$

$$\mathbf{E}_2(t) = \frac{E_0}{2}\sin(\omega t)(\mathbf{n}_h - \mathbf{n}_v)$$

which then traverse their respective arms and arrive back at the beam splitter with a phase offset, ωτ, that depends on the path length difference

$$\mathbf{E}_1(t) = \frac{E_0}{2}\sin(\omega t - \omega\tau)(\mathbf{n}_h + \mathbf{n}_v)$$

$$\mathbf{E}_2(t) = \frac{E_0}{2}\sin(\omega t)(\mathbf{n}_h - \mathbf{n}_v)$$

The path length difference is controlled by a motorized stage on which is mounted one of the roof mirrors. The right angle roof mirrors adjust the polarization of the light such that what got transmitted(reflected) at the splitter now gets reflected(transmitted) so that it can be properly recombined into

$$\mathbf{E}(t,\tau) = \frac{E_0}{2}\left[\left(\sin(\omega t - \omega\tau) + \sin(\omega\tau)\right)\mathbf{n}_h + \left(\sin(\omega t - \omega\tau) - \sin(\omega\tau)\right)\mathbf{n}_v\right]$$

The recombined wave is then focused and split into horizontal and vertical polarizations, each of which are directed to a pyroelectric detector. The average intensity seen by each detector is

$$I_{h,v}(\omega,\tau) \propto \lim_{T\to\infty} \frac{1}{2T}\int_{-T}^{T} dt\,\left(\mathbf{E}(t,\tau)\cdot\mathbf{n}_{h,v}\right)^2$$

$$I_h(\omega,\tau) \propto \frac{E_0^2}{2}\cos^2\left(\frac{\omega\tau}{2}\right)$$

$$I_v(\omega,\tau) \propto \frac{E_0^2}{2}\sin^2\left(\frac{\omega\tau}{2}\right)$$

The sum of the intensities seen by the two detectors is proportional to the total intensity after the initial input polarizer. Defining the interferogram, $S(\tau)$, to be the intensity difference divided by the sum results in

$$S(\omega,\tau) = \cos(\omega\tau)$$

This result is for a single frequency, ω, but can be generalized to an arbitrary wave by Fourier composition. The intensities are then integrals over frequency space and the interferogram is

$$S(\tau) = \frac{\int d\omega\, I(\omega)\cos(\omega\tau)}{\int d\omega\, I(\omega)}$$

which is the real part of the Fourier Transform of $I(\omega)$. Inverting this gives

$$I(\omega) = \left|\Re\left[\mathbf{F}^{-1}\{S(\tau)\}\right]\right| \qquad (4)$$

where $\Re$ denotes the real part of a complex number, and $\mathbf{F}^{-1}\{\}$ indicates an inverse Fourier Transform.

The intensity outputs, $I_{h,v}$, of the pyroelectric detectors are attached to an oscilloscope from which the peak values from an average over 8 macropulses are obtained. The mirror position is set via a hand controller.

ANALYSIS

Several interferograms were taken over the course of 3 days. Figure 7 shows the interferogram and corresponding frequency spectrum from the 3rd day which used the widest path difference window. The interferometer is contained in an enclosure through which dry nitrogen can be flowed. For this particular sample, N_2 flowed for ~16 hours before taking data.

From Equation 2, $F(0) = 1$, and since the charge density is always positive, $F(0)$ is the upper bound on the magnitude of the spectrum. Because the detection system has a variety of low frequency cutoffs, the measured spectrum does not go to 1 at zero frequency. One way around this problem is to replace the low frequency region with a curve that goes smoothly to 1 at $\omega = 0$. The simplest curve to have this property is a parabola. Figure 8 shows both the raw and corrected spectra using a parabolic fit to

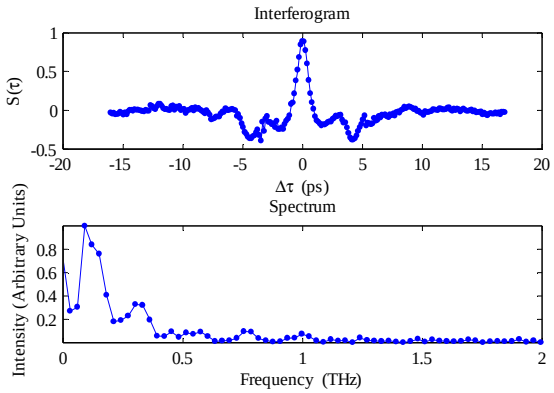

Figure 7: Interferogram (Top) and measured spectrum (Bottom) from compressed beam. One can see what appears to be interference fringes in the spectrum with a period of ~0.2 THz corresponding to 1.5 mm wavelength. This is comparable to what was measured by [9].

the 4th -8th points in the spectrum and replacing the first 3 points with the values of the parabola. To extract the bunch profile, Equations 2, 3, and 4 are combined to give

$$\rho(t) \propto \mathbf{F}^{-1}\left\{ \left|\sqrt{I(\omega)}\right| e^{\,i\frac{2\omega}{\pi}\int_0^\infty d\omega' \frac{\ln\left|\sqrt{I(\omega)}\right| - \ln\left|\sqrt{I(\omega')}\right|}{\omega^2-\omega'^2}} \right\}$$

from which the bottom plot in Figure 8 is obtained.

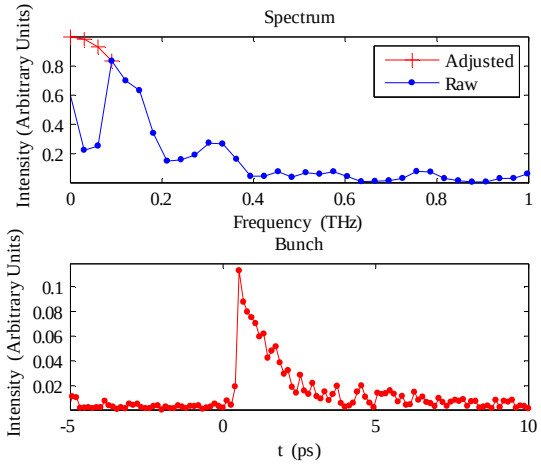

Figure 8: Top) Raw and adjusted spectra. The adjusted spectrum is the raw spectrum with the lowest 3 points replaced by the parabolic extrapolation values. Bottom) The bunch distribution in ps.

To obtain the bunch length, the width of the distribution in Figure 8 should be corrected for the diffraction effect. Since the width is under 1 ps, the diffraction correction from Figure 4 is fairly small (<5%).

To get a handle on systematic uncertainties, one can perform some conservative variations such as not adjusting the spectrum, or filling in the interference bumps in the spectrum (see Fig. 9). Table 1 lists these variations and the effect on the bunch length.

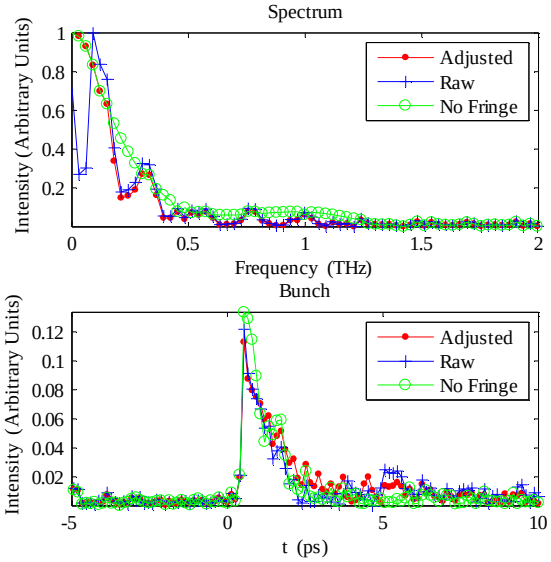

Figure 9: Impact on the bunch length of various corrections to the spectrum.

Table 1: Change in the bunch length with changes in the analysis techniques.

Technique	**Bunch Length (FWHM)**
Spectrum Adjusted	0.9 ± 0.1 ps
Raw Spectrum	0.8 ± 0.1 ps
Fringe Removal	0.7 ± 0.1 ps

A measurement without compression was also taken as shown in Figure 10. This measurement is difficult due to the fact that the spectrum is dominated by contributions in the poorly measured region below 200 GHz where the spectral response of the experimental setup is the main contributor to the shape. The measured width is ~3 ps. After correcting for diffraction, the FWHM bunch length is 3.3 ps.

Some items missing from the analysis are effects from diffraction of the optical elements, wakefields, water vapour, and interference in the pyroelectric detectors [9] and quartz window.

FUTURE

Currently, the interferometer is being reinstalled in a new beamline at the photoinjector. The chicane has been replaced with a double dogleg for an emittance exchange experiment. The interferometer will be after the second dogleg and shares a port with a streak camera which can be used for calibration purposes. The DAQ and mirror control is being automated which should allow for more regular measurements. New pyroelectric detectors with reduced interference have been obtained and there is the possibility of using broadband schottky diode antenna detectors in place of the pyroelectric detectors.

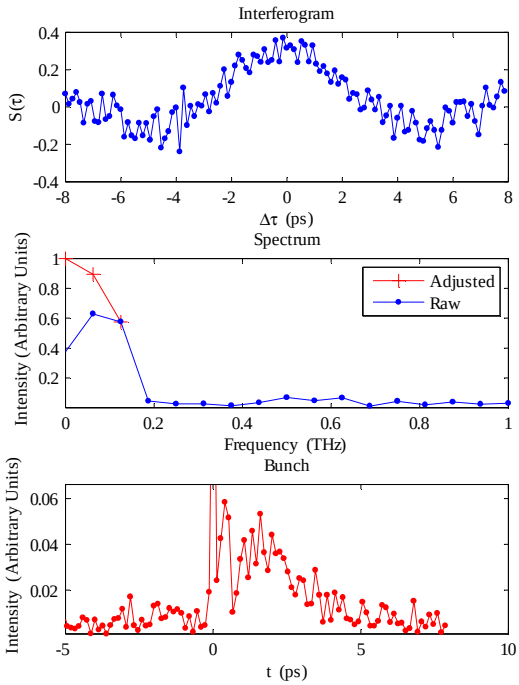

Figure 10: Top) Uncompressed beam interferogram. The window was probably not wide enough to obtain reliable results. Middle) Raw and adjusted spectra. Because beam is uncompressed, the spectrum is dominated by the poorly measured region. Bottom) Bunch distribution.

ACKNOWLEDGEMENTS

We would like to thank J. Santucci, C. Lundberg, and J. Ruan for their assistance in installing and aligning the interferometer. Also D. Milhalcea for discussions about bunch length interferometry.

REFERENCES

[1] S. Dobert *et al.*, Accelconf/e 96.
[2] P. Evtushenko *et al.*, THPPH064, Proceedings of FEL 2006.
[3] D. Mihalcea *et al.*, PRST-AB V **9**, 082801 (2006).
[4] V.L Ginzburg and I.M. Frank, J. Exp. and Theoret. Phys., Vol. 16, pp. 15-21, 1946.
[5] L. Frohlich, "Bunch length measurements using a Martin-Puplett interferometer at the VUV-FEL", DESY-THESIS-2005-011, DESY-TESLA-FEL-2005-02, Jun 2005. 60pp.
[6] M. Castellano and V.A. Verzilov, PRST-AB V **1**, 062801, (1998).
[7] R. A. Bosch, PRST-AB, V **5**, 020701 (2002).
[8] G. Kazakevich et al., TUPPH015, Proceedings of FEL 2007.
[9] C. Settakorn, H. Wiedemann, (APAC '01), Beijing, China, 17-21 Sep 2001. Published in 2nd Asian Particle Accelerator Conference 728.